Rover Publications
United International Journal of Engineering and Sciences (UIJES)
An International Peer-Reviewed Engineering and Science Journal;Impact Factor: 5.735(SJIF)
www.uijes.com Vol-3,Issue-3 ,2022 ISSN:2582-5887

Structural, Optical & Thermal Properties of a Host Crystal Lattice and to Explore its Inherent Possibilities

1.Sanjay Kumar Dubey,2.Shashank Sharma

1.Assistant Professor, Department of Physics, Dr. Radha Bai, Govt. Navin Girls College, Raipur (C.G.), India

2.Assistant Professor, Department of Physics, Dr. C. V. Raman University, Kota, Bilaspur (C.G.), India

Abstract

Host $Ba_2MgSi_2O_7$ phosphor was successfully prepared via low temperature combustion synthesis route. The phase identification of the prepared phosphor was done with the help of powder XRD technique. The XRD pattern of the phosphor revealed its monoclinic crystal symmetry with a space group C2/c. XRD pattern of synthesized powder sample have well-matched with the help of JCPDS PDF Card No. #23-0842. The average crystallite size calculated as 44nm with the help of Debye Scherer's mathematical formula and also calculated as 56nm using Williamson–Hall (W–H) plot method and crystal lattice strain has been calculated as 0.24nm. This Raman line corresponds to the stretching vibrations of the Si–O bonds of the Si_2O_7 group. It is acquired that the sample exposed for 15min gives optimum TL intensity at 112.19^0C temperature and displays single TL glow peak. On the basis of TL glow curve, it can be suggested that the $Ba_2MgSi_2O_7$ (BMS) phosphor is an efficient host lattice but not a better TL phosphor. In thermo-luminescence property, the effect of 15min UV exposure on different kinetic parameters for this peak was determined with the help of peak shape method. In our present study, we have studied on the XRD, FESEM, Raman & IR Spectra and thermo-luminescence (TL) characteristics of this phosphor.

Keywords: *X-ray diffraction (XRD), $Ba_2MgSi_2O_7$ (BMS), Raman Spectra, Monoclinic, C2/c*.

1. Introduction

Since, 21^{th} century, national progress was closely linked with scientifically and technologically development and that linkage intensified in last few decades. The nano materialistic research achievement is more important and necessary role in the progressive and development of technological era. Our new innovative rare earth do-pant ions such as Eu, Er, Tb, Dy and Ce are more essential part in our advanced materialistic achievements of optical display system lightening LEDs. But the biggest challenge is finding a worthy host crystal lattice. Green nature inspired manufacturing technologies for sustainable developments are the key issues that environmental biomaterial addresses. Thermo Kinetic parameters are an essential analytic part that many applications in nanomaterials and high temperature dosimetry radiation. It concerned with thermally stimulation process that can be initiated by changing temperature. Emerging technologies and nano applications that demand advanced, high-tech

innovative materials like silicates, aluminates, sulphides to highly approach studied. Biomaterials literally means a living organism bio active molecule in vitro and vivo, used in tissue engineering [1]. Various characterization methods for all prepared samples were utilized to brief investigation of the phase structure, average particle size and surface morphology. Inorganic solid-state silicates have become a focus of technological interest due to their favorable physical and chemical properties. For variety of applications, various silicates host materials doped with rare-earth and other ions have been widely investigated as luminescent materials. The best long persistent phosphor known till now is $SrAl_2O_4$: Eu^{2+}, Dy^{3+} which is a commercial phosphor and may have afterglow for more than 20 hours [2,3]. Many of the silicate based phosphors doped with divalent or trivalent rare-earth ions likewise Eu^{2+}, Dy^{3+}, Ce^{3+}, Er^{3+} have been preferred for used as commercial phosphor in fluorescent lamp, scintillators [4,5], plasma display panels, white light emitting diodes (WLEDs), long persistent phosphor, high temperature radiation dosimetry applications. In monoclinic $Ba_2MgSi_2O_7$ crystal structure have been clearly displayed octahedral [BaO_8] sites because the octahedral coordination number of Ba^{2+} ion and tetrahedral for both Mg^{2+} and Si^{4+} ions [6]. Dubey et al. proposed that the $Ba_2MgSi_2O_7$ has revealed a monoclinic structure with space group C2/c [7]. Our only intension behind this present research investigation is to find out the possibility of better performance in a suitable host crystal lattice, as the selection of a better host material is what drives the entrepreneurship of the main characteristics (such as structural, and thermal) of any phosphor. In this paper, host $Ba_2MgSi_2O_7$ sample was successfully synthesized via combustion synthesis technique and its structural properties such as XRD, FESEM and optical properties such as Raman Spectra as well as thermal characteristics such as thermoluminescence (TL) spectra have also be briefly discussed.

2. Experimental Studies

2.1 Sample Preparation

It is a very large group family of compounds which characterized through the general composition formula like $M_2X^1Y^2{}_2O_7$, [where M; denotes Ba, Sr & Ca, X^1; denotes Mg, Zn, Cu, Mn & Co and Y^2; denotes Ge & Si]. The compounds of this group are being widely intensive studies as optical materials [8]. Low temperature combustion synthesis route is one of the best synthesization routes as compared to other synthesis techniques. In this technique, very low heating temperature and less time for synthesization are required. We applied in our experiment; $Ba_2MgSi_2O_7$ (BMS) were successfully synthesized via Low temperature combustion synthesis route. As starting materials, for the synthesization of host $Ba_2MgSi_2O_7$ sample, Analytical grade Ba $(NO_3)_2$ (99.99%), Mg $(NO_3)_2$ (99.99%), SiO_2*H_2O (99.99%), NH_2CONH_2 (99.99%) (Urea) and H_3BO_3 (99.99%) were used in our present investigation study. The precursor chemicals were taken according to their respective stoichiometric ratio required for the preparation of desired phosphor and mixed in a mortar pestle. Urea (NH_2CONH_2) has been used as a combustion fuel and boric acid (H_3BO_3) also employed as an oxidizer or flux. The stoichiometric ratio of the precursor powders specimens using with acetone (CH_3COCH_3) were grinded thoroughly in an agate mortar-pestle before being transferred to a cylindrical silica crucible. Then the mixture was fired at 650^{o}C in muffle furnace. The mixture undergoes thermal dehydration and ignites at 1000^{0}C for 1h with liberation of gaseous products, to yield silicates. The entire combustion process was completed in about 5min. The products obtained by combustion process were fluffy masses and after additional crushing converted into a fine powder. The

resulting sample was restored in airtight bottle for structural and optical characterization studies [10]. The sintered BMS sample was obtained as an optically translucent (i.e. semi-transparent) and white (i.e. colorless) powder.

The chemical reaction of this process is given as follows:

$$Ba\ (NO_3)_2 + Mg\ (NO_3)_2 + SiO_2{*}H_2O + NH_2CONH_2 + H_3BO_3 \rightarrow Ba_2MgSi_2O_7 + H_2O\ (\uparrow) + CO_2\ (\uparrow) + N_2\ (\uparrow) \quad (1)$$

For the combustion process of oxides, metal nitrates are applied as oxidizer and urea is also applied as a reducer [9]. With the calculation of oxidizer to fuel ratio, the elements were assigned formal valences as follows: Ba = +2, Mg = +2, Si = +4, B = +3, C = +4, H = +1, O= -2 and N = 0. Thus, the heat of combustion is maximum for Oxidizer/Fuel ratio is equal to 1 [10].

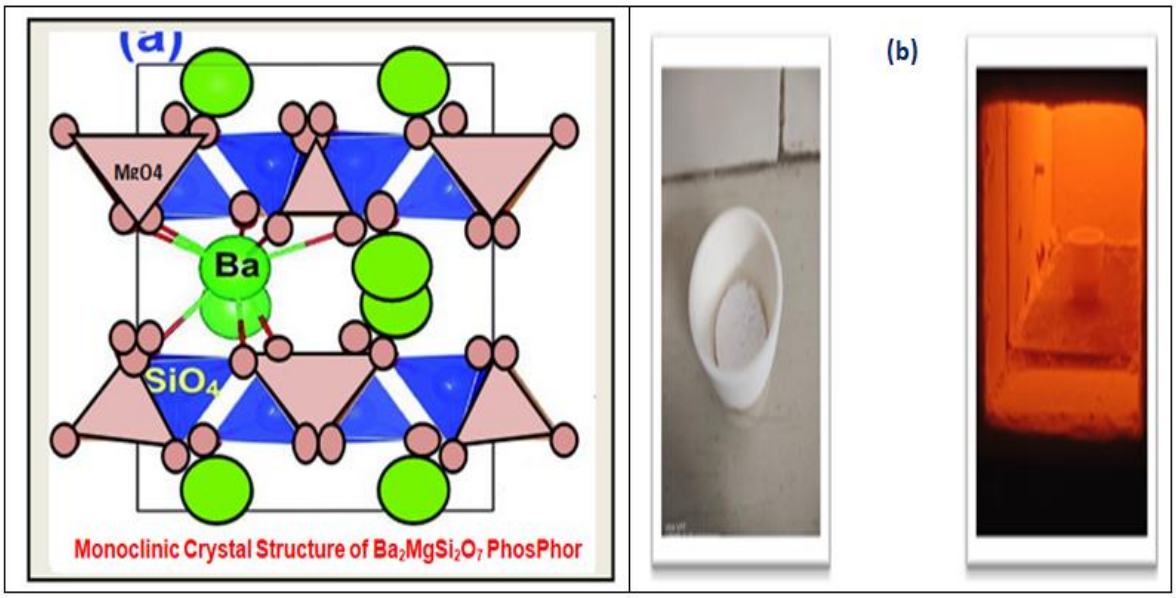

Fig. 1 [a] Monoclinic Crystal Structure and [b] Prepared Pure $Ba_2MgSi_2O_7$ Sample

2.2 Sample Characterization

XRD of the crystalline structure, size and phase composition of the synthesized phosphor were noted with the help of Bruker D8 advance X-ray diffractometer with Cu-K_α radiation having wavelength (λ = 1.5405Å), at 40 kV, and 40 mA voltage and current values, respectively. Surface morphology of the sample was examined with the help of SEM (ZEISS model microscope). Raman & IR spectra have been characterized with the help of Centre India Raman Spectrometer. A routine Thermo-luminescence (TL) study of the UV-irradiated (254 nm) samples was recorded with the help of routine TL set-up Nucleonix TL 1009I TLD reader (Integral-PC Based) with constant heating rate 5^0Cs^{-1}. All experiments were performed in identical conditions. All experiments were performed in identical conditions, and it was observed that the results were reproducible. All measurements carried out in the room temperature.

3. Results and Discussion

3.1 XRD Analysis

XRD patterns were recorded in the range between (10^0\2θ\$80^0$) of un-doped $Ba_2MgSi_2O_7$ powder sample was successfully synthesized by combustion synthesis route. All the peaks have been displayed according to the standard JCPDS PDF file No. 23-0842 [11]. The cell volume the following lattice parameters were also examined [12]. All parameters have shown in Table no. 1. We have suggested that the di barium magnesium di silicate [$Ba_2MgSi_2O_7$] sample is better host material. Few extra peaks were displayed in the XRD patterns. XRD diffraction peaks were peaked at (15.35), (22.42), (25.25), (26.88), (27.51), (29.22), (31.16), (32.69), (34.92), (44.14), (47.39), and (54.14) corresponding to (020), (002), (202), (112), (022), (131), (222), (113), (310), (114), (151), and (153) planes respectively and Sharper and isolated XRD peaks likewise 2θ = 22.42 (002), 27.51 (022), 29.22 (131), 31.16 (222), 32.69 (113), 54.14 (153) were chosen for crystallite size evaluation. The relevant crystallite size is ~ 40nm, 48nm, 42nm, 46nm, 44nm, 44nm was evaluated with the help of the Debye-Scherrer's formula respectively and the average crystallite size is obtained ~ 44nm. The XRD pattern confirms that the pure phase of monoclinic $Ba_2MgSi_2O_7$ formed at an annealing temperature of 1000^0C for 1h.

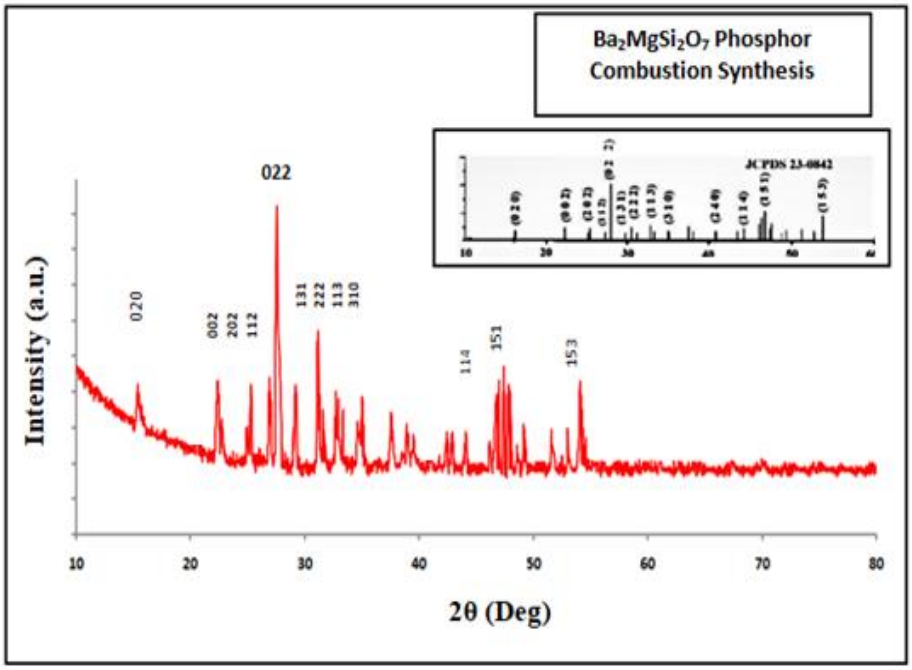

Fig. 2 XRD Pattern of Synthesized $Ba_2MgSi_2O_7$ Phosphor

3.1.1 Debay-Scherrer formula

To determine the crystallite size (D), using Debye–Scherrer empirical formula is represented as follows:

$$D = \frac{k\lambda}{\beta Cos\theta} \qquad (2)$$

Where k = 0.94 (Scherrer constant), λ is wavelength of occurrence X-ray (for Cu-Kα radiation, λ = 1.5406 Å), β is the FWHM (Full width half maximum) of the peaks and θ (theta) is presented the corresponding Braggs diffraction angle [13] as well as D denotes crystallite size. The lattice parameters (in Table No. 1) of sintered powder sample, which have observed according to prominent peak (022), position of the peak of the XRD patterns and the calculation values of parameters.

Table: (1) Lattice Parameters of Synthesized Pure $Ba_2MgSi_2O_7$ Phosphor

No.	Lattice Parameters	Properties
1.	Crystal Structure	Monoclinic
2.	Space Group	C2/c
3.	Lattice Parameters	a = 8.4128 Å, b=10.7101 Å, c = 8.4387 Å & $\alpha=90^0$, $\beta=110.71°$ $\gamma=90^0$
4.	Cell Volume	711 $(Å)^3$
5.	Radiation	Cu-Kα 1
6.	Incident X-ray Wavelength	1.5406 Å

3.1.2 Williamson-Hall (W-H) Plot Method of Analysis

This method clearly based on Uniform Deformation Model (UDM). Using this method, we obtain the graph between βCosθ and 4Sinθ. Fig. 3 displays the W-H plot of the various diffraction peaks of BMS phosphor. The Williamson-Hall (W-H) method is one of the best methods to consider the effect of strain-induced X-ray diffraction [XRD] peak extension. In addition, this method provides the calculation of the intrinsic strain as well as crystalline size [14,15].

This method is seen as a very important and very useful method from the point of view of estimating the crystal lattice strain clearly present in the synthesized samples. In this way, FWHM can be represented as a linear combination of the major role from the crystallite size & crystal lattice strain [16]. The crystal lattice strain induced broadening in the powder material was calculated via the following mathematical relation given as below:

$$\beta\cos\theta = \frac{k\lambda}{D} + 4\varepsilon \sin\theta \qquad (4)$$

Where, 'β= 2 (θ_2- θ_1)'; indicates the FWHM (in radians), 'θ' indicates the Bragg angle of the peak, 'λ' (i.e. 1.5405 Å); indicates the wavelength of X-ray used, 'D'; indicates the effective particle size and 'ε'; indicates the effective crystal lattice strain [17].

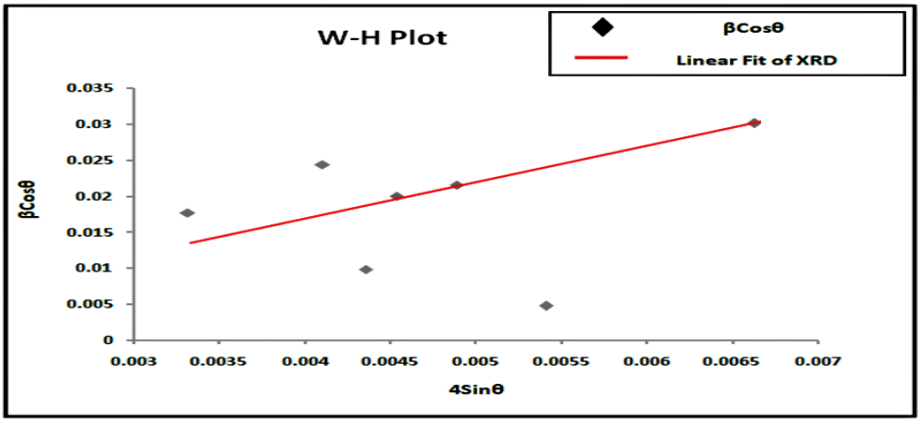

Fig. 3 Williamson-Hall Plot of Pure $Ba_2MgSi_2O_7$ Phosphor

The determination of the effective particle size [D] for which the crystal lattice strain is taken into account can be the extrapolated from the plot as clearly displayed in Fig.3. The crystal lattice strain was determined from the slope and the crystalline size was determined from the y-intercept of the linear fit. The W-H plots clearly demonstrate that the line extension was essentially isotropic, which indicates that the diffraction domains were isotropic and present with a small percentage of microscopic-strain. Sharper and isolated XRD peaks likewise 2θ = 22.42 (002), 27.51 (022), 29.22 (131), 31.16 (222), 32.69 (113), 54.14 (153) were chosen for crystallite size and crystal lattice strain evaluation. The relevant crystallite size is ~ 56nm, 60nm, 52nm, 58nm, 56nm, 54nm was evaluated with the help of the W-H plot method respectively and the average crystallite size is obtained ~ 56nm and crystal lattice strain is obtained as ~0.24nm.

The average crystallite size calculated as 44nm with the help of Debye Scherer's mathematical formula and also calculated as 56nm using Williamson–Hall (W–H) plot method. The average crystal size and of all synthesized samples was obtained to be maximum value calculated by W-H plot method as compared to the Debye scherrer method.

Table: 2 Determinations of Average Crystallite Size and Lattice Strain Size

Diffraction Angle	Respective Plane	Debye Scherer's Formula (nm)	W-H Plots Method (nm)	Lattice Strain Size (nm)
22.42	002	40	56	0.23
27.57	022	48	60	0.24
29.22	131	42	52	0.25
31.16	222	46	58	0.24
32.69	113	44	56	0.24
54.14	153	44	54	0.25
Average size		~44nm	~56nm	0.24nm

3.2 FESEM Analysis

In Fig. 4, the surface morphology of the prepared nano phosphor is displayed in 30.00 K X magnification with 1μm nano range. A closer examination of the FESEM image demonstrates that the particle's surface morphology was not uniform and at the same time they were very tightly clustered with each other to form numerous secondary particles [18]. One of the FESEM image represents that the all samples have smooth and homogeneous crystal structure with isolated pores. From the FESEM image, it can be clearly examined that the particles with different size distributions are present in prepared samples. Furthermore, these samples have been prepared by low temperature heat-treatment, due to which there are some large aggregates exist in them.

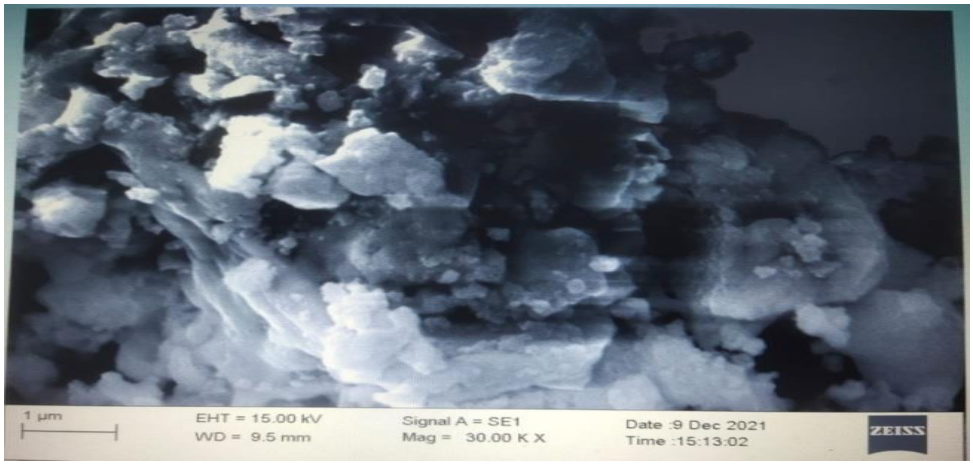

Fig. 4 FESEM Image of Pure $Ba_2MgSi_2O_7$ Phosphor

3.3 Raman and IR spectra

It is a special type of analytical technique, where scattered light is better utilized to measurement the vibrational energy modes of a specimen, called as Raman spectroscopy [19]. The phonon energy of materials can be characterized via Raman spectroscopy. The Raman spectrum of pure $Ba_2MgSi_2O_7$ sample phosphor is represented in Fig. 5(a). To ensure the single phase of the phosphor powder, $Ba_2MgSi_2O_7$ samples annealed at 1000^0C for 1h were subjected to Raman scattering measurements, which have taken at room temperature. The Raman spectrum of the $Ba_2MgSi_2O_7$ sample presents huge Raman shifts at about 147, 179, 235, 289, 448, 658, 895, and 969cm^{-1}. The lines correspond to the stretching vibrations of the Si–O bonds of the Si_2O_7 group [20,21]. The IR spectra [fig. 5 (b)] are similar to those previously published. The unit cell volume and Si-O-Si angle depend on the absorption wavelength. These results suggest that no peak shift occurred $Ba_2MgSi_2O_7$ peaks.

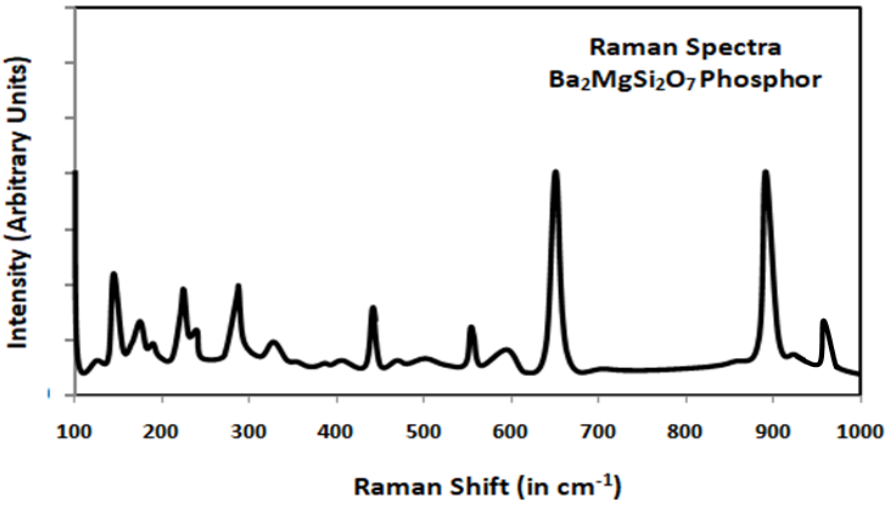

Fig. 5 [a] Raman Spectra of Pure $Ba_2MgSi_2O_7$ Phosphor

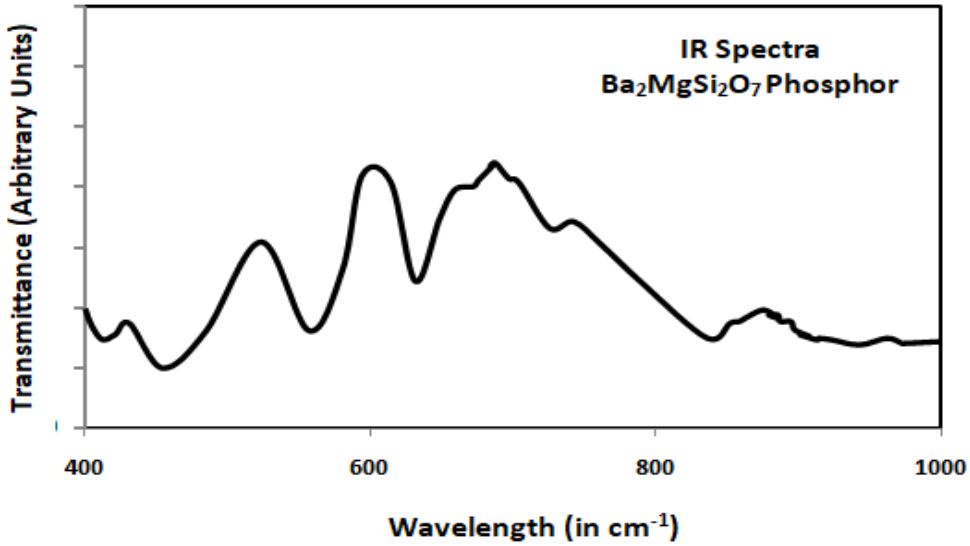

Fig. 5 [b] IR Spectra of Pure $Ba_2MgSi_2O_7$ Phosphor

3.4 Thermo-luminescence (TL) Study

Thermo-luminescence phosphor display afterglow characteristics, which are known as persistent luminescence, and they are very needful in various field of applications likewise brightness in the darkness road, bio-imaging and emergency sign. At present time, the evolution of novel TL materials demonstrates a new and rapid developing application of research in physics, medicine area as well as mineral prospering, archaeological dating, forensic science and high temperature radiation dosimetry [22].

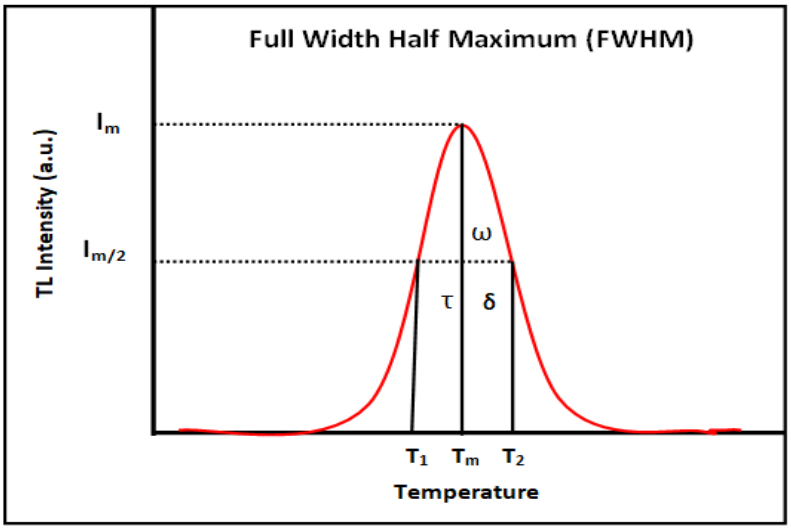

Fig. 6 FWHM of Glow Curve

From the TL glow curve, it is seen that, initially thermo-luminescence [TL] intensity increase with increasing UV irradiation time. The optimum TL intensity is maximum for 15 min of UV exposure, after that they start to decrease. It is predicted that with the increasing UV irradiation time, large amount of charge carriers are released which increases the trap density results in increase of TL intensity (density of charge carrier may have been increasing), but after a specific exposure (15 min) traps density starts to destroy results in decrease in TL intensity [23].

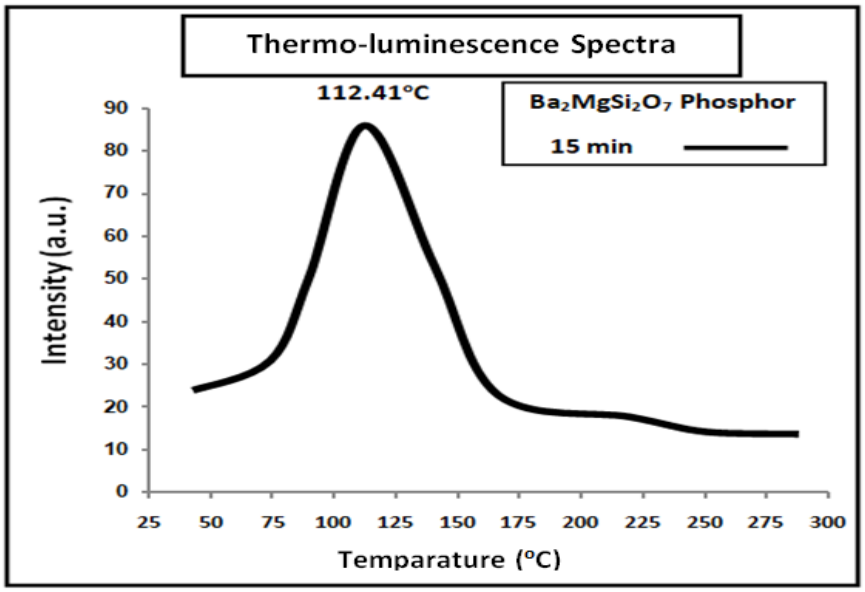

Fig. 7 TL Glow Curve of Pure $Ba_2MgSi_2O_7$ Phosphor with 15 min UV irradiation Time

Fig. 7 displays that the single TL glow curve of $Ba_2MgSi_2O_7$ phosphor has been obtained with 15min UV irradiation time at constant heating rate 5^oCs^{-1}. For TL measurement, the fixed amount of the powder specimens were kept (8mg) in cavity. The TL glow curve peak was allocated at 112.41°C temperature respectively, and these peak positions remains constant with UV irradiation time. In our case, the TL peak is very weak and can be neglected. Observing the TL glow curve, we find that the maximum glow curve is obtained at 112.41°C. From 68.45°C temperature, TL intensity is continuously increasing up to 112.41°C. Thereafter that the TL intensity is decreasing continuously up to 168.37°C temperature. Thereafter TL intensity curve is near about flate and constant having the lowest value of TL intensity up to 300°C temperature.

3.3.1 Calculation of Kinetic Parameters

The thermo-luminescence (TL) characteristics of a phosphor mainly depends on the kinetic parameters i.e. Trap-depth or activation energy (E), order of kinetics (b), and the frequency factor (s) describing the trapping emitting centers which is quantitatively responsible for the thermo-luminescence (TL) emission. TL phosphors exhibit glow curves with one or more peaks when the charge carriers are released. There are various methods for determining the kinetic parameters from TL glow curves. For example, when one of the TL glow peaks is highly isolated from the others, the experimental technique such as peak shape method [fig. 6] is appropriate to determine kinetic parameters. The TL parameters for the prominent glow peak of sintered phosphor were calculated with the help the peak shape method [24,25].

[a] Order of Kinetics [b]

It clearly depends on the peak shape of TL glow curve. The mechanism of recombination of de-trapped charge carriers with their counterparts is called as the order of kinetics [b]. The kinetic order for glow peak of $Ba_2MgSi_2O_7$ phosphor can be determined via calculating geometrical factor μ_g from the mathematical relation as follows:

$$\mu_g = \frac{\delta}{\omega} = \frac{T_2 - T_m}{T_2 - T_1} \qquad (2)$$

Where T_m is the optimum peak temperature, T_1 and T_2 are temperatures at half intensity on the ascending and descending parts of the glow peak, respectively, [$\omega = T_2 - T_1$], the high-temperature half width [$\delta = T_2 - T_m$]. The geometric factor is to differentiate between first and second order TL glow peak. [μ_g = 0.39-0.42] for the first order kinetics; [μ_g = 0.49-0.52] for the second order kinetics and [μ_g = 0.43-0.48] for the mixed order kinetics [26].

[b] Activation energy (E)

The activation energy [E] or trap depth can be determined by the general formula, which is valid for any kinetics. It is given by mathematical relation as follows:

$$E_\alpha = C_\alpha\left(\frac{kT_m^2}{\alpha}\right) - b_\alpha(2kT_m) \qquad (3)$$

For general order kinetics, the values of the C_α and b_α ($\alpha = \tau, \delta, \omega$) are expressed as $c_\tau = [1.51 + 3(\mu_g - 4.2)$, $b_\tau = [1.58 + 0.42((\mu_g - 0.42)]$; $c_\delta = [0.976 + 7.3(\mu_g - 0.42)]$, $b_\delta = 0$ and $c_\omega = [2.52 + 10.2(\mu_g - 0.42)]$, $b_\omega = 1.0$.

[c] Frequency factor

It's clearly reflecting the probability of electron escape from the traps after exposure to ionizing radiation. Frequency factor is one of the most significant parameters for material characterization. After obtaining the order of kinetics [b] and activation energy [E], the frequency factor [s] can be determined with the help of the following mathematical relation through replacing the values of E and b [26,27]:

$$\frac{\beta E}{kT_m^2} = s\left[1 + (b-1)\frac{2kT_m}{E}\right]\exp(-E/kT_m) \qquad (4)$$

Where k is Boltzmann constant, E is activation energy, b is an order of kinetics, T_m is a temperature of peak position, and β is the heating rate. In the present work $\beta = 5^0 Cs^{-1}$.

The kinetic parameters were evaluated with the help of the thermo-luminescence (TL) glow curve of prepared pure powder sample with different UV irradiation time at constant heating rate 5^oCs^{-1} has been displayed and summarized in Table 3.

Table: 3 The Kinetic Parameters for UV Irradiated Pure $Ba_2MgSi_2O_7$ Phosphor

UV min	HTR	T_1 (^oC)	T_m (^oC)	T_2 (^oC)	τ	$^{\delta}$	ω	$\mu = {}^{\delta}/\omega$	E (eV)	Frequency Factor (s^{-1})
15	5^oCs^{-1}	82.45	112.41	139.28	29.96	26.87	56.83	0.47	0.57	7.8×10^7

For pure $Ba_2MgSi_2O_7$phosphor, geometric shape factor (μ_g) is calculated to be 0.47. The corresponding Activation energy (E) and frequency factor (s^{-1}) were evaluated as 0.57 eV and 7.8 ×

$10^7 s^{-1}$ respectively. In our experiments, shape factor (μ_g) is a lie between (0.43-0.48), which indicates that it is a case of mixed order kinetics. It is very close to second order kinetics. In our case, the thermo-luminescence [TL] peak of this phosphor is very weak because on heating the sample, the charge carriers leave their valance band and move towards the conduction band, and thus return straight back without falling into any trap there. The result is that the TL intensity is not that high. For this reason, we need doping of a suitable do-pant rare earth ions in the host crystal lattice site for trap construction. Because the do-pant ions generate a trap in the host crystal lattice site in which the charge carriers get trapped there. That is, the charge carriers trapped in the trap take more time to return from there, due to which their TL intensity increases.

Conclusion

In summary, Undoped $Ba_2MgSi_2O_7$ (BMS) phosphor sample was successfully synthesized via low temperature combustion synthesis route and its XRD, FESEM, Raman spectra and thermo-luminescence (TL) properties were also investigated. The analysis of XRD patterns revealed that the single-phase monoclinic crystal structure of synthesized phosphor was confirmed. The average crystal size and of all synthesized samples was obtained to be maximum value calculated by W-H plot method as compared to the Debye scherrer method. The grains size of the sintered phosphor in nano range and homogeneity much better. The Raman spectrum of the synthesized $Ba_2MgSi_2O_7$ sample presents huge Raman shifts at different wave numbers. These lines correspond to the stretching vibrations of the Si–O bonds of the Si_2O_7 group. On the basis of comparison of TL results, we can say that the host $Ba_2MgSi_2O_7$ phosphor has been shown thermal spectra at comparatively very low TL intensities. After this overall study, it would be fair to say that the TL intensities do not achieve their optimal level due to the large band gap in the host materials. This is the reason why doping process should be adopted to narrowband gap so that TL glow curves can be obtained at higher intensities.

Acknowledgements

We gratefully acknowledge to the kind support for the facility of XRD, FESEM and Raman spectral analysis, NIT Raipur (C.G.). Authors are also thankful to Pt. Ravishankar Shukla University, Raipur (C.G.) for providing us the facility of thermoluminescence analysis. We are also heartily grateful to Dept. of physics, Dr. Radha Bai, Govt. Navin Girls College Mathpara Raipur (C.G.), providing the facility of muffle furnace and other essential research instruments.

Conflict of Interest

There is no any conflict or any economic interest that exists in our present research work.

Funding Sources

The authors have not received any finacial support for the research work, authorship and/or publication of this research article.

Authors Contribution

This work was carried out in collaboration between both authors. Author Dr. Shashank Sharma undertakes the manuscript designed and conducted the entire experiments & characterization studies, collected and analyzed the research data, and prepared the entire manuscript draft as well as supervised the results-discussion. Similarly, author Dr. Sanjay Kumar Dubey has properly checked the spelling mistake, punctuation, grammatical error and helped in sample preparation. Both authors read and approved the final manuscript.

References

[1] Bhatkar, V. B., & Bhatkar, N. V. (2011), Combustion synthesis and photoluminescence study of silicate biomaterials. *Bulletin of Materials Science*, *34*(6), 1281-1284.

[2] Garlick, G. F. J., & Gibson, A. F. (1948). The electrons trap mechanism of luminescence in sulphide and silicate phosphors. *Proceedings of the Physical Society (1926-1948)*, *60*(6), 574.

[3] Van den Eeckhout, K., Smet, P. F., & Poelman, D. (2010). Persistent luminescence in Eu2+-doped compounds: a review. *Materials*, *3*(4), 2536-2566.

[4] Kamiya, S., & Mizuno, H. (1999). Phosphors for lamps. *Phosphor Handbook*, *2*.

[5] Aitasalo, T. U. O. M. A. S., Holsa, J., Laamanen, T. A. N. E. L. I., Lastusaari, M. I. K. A., Lehto, L. A. U. R. A., Niittykoski, J. A. N. N. E., & Pelle, F. A. B. I. E. N. N. E. (2005). Luminescence properties of Eu^{2+} doped dibarium magnesium disilicate,$Ba_2MgSi_2O_7$:Eu^{2+}. *Ceramics-Silikaty*, *49*(1), 58-62.

[6] Komeno, A., Uematsu, K., Toda, K., & Sato, M. (2006). VUV properties of Eu-doped alkaline earth magnesium silicate. *Journal of alloys and compounds*, *408*, 871-874.

[7] Dubey, SK, Sharma S., Diwakar AK, Pandey, S. (2021). Synthesization of Monoclinic ($Ba_2MgSi_2O_7$: Dy^{3+}) Structure by Combustion Route. *Journal of Materials Science Research and Reviews,* 8, 172-179.

[8] Sharma, S., & Dubey, S. K. (2021). The significant properties of silicate based luminescent nanomaterials in various fields of applications: a review. *International Journal of Scientific Research in Physics and Applied Sciences*, *9*(4), 37-41.

[9] Ekambaram, S., & Maaza, M. (2005). Combustion synthesis and luminescent properties of Eu^{3+}-activated cheap red phosphors. *Journal of alloys and compounds*, *395*(1-2), 132-134.
Kingsley, J. J., & Patil, K. C. (1988). A novel combustion process for the synthesis of fine particle α-alumina and related oxide materials. *Materials letters*, *6*(11-12), 427-432.

[10] JCPDS Pdf file number 23-0842, JCPDS *International Center for Diffraction Data*.

[11] Aitasalo, T., Hölsä, J., Laamanen, T., Lastusaari, M., Lehto, L., Niittykoski, J., & Pellé, F. (2006). Crystal structure of the monoclinic $Ba_2MgSi_2O_7$ persistent luminescence material. *Zeitschrift fur Kristallographie Supplements*, *2006*, 481-486.

[12] Sharma, S., Kumar Dubey, S., K Diwakar, A., & Pandey, S. (2021). Novel White Light Emitting ($Ca_2MgSi_2O_7$: Dy^{3+}) Phosphor. *Journal of Material Science Research and Reviews,* 8(4), 164-171.

[13] Jacob, R., & Isac, J. (2015). X-ray diffraction line profile analysis of BaSr0. 6Fe0. 4TiO3 [BSFTO]. *Int. J. Chem. Studies*, *2*(5), 12-21.

[14] Warren, B. E., & Averbach, B. L. (1952). The separation of cold-work distortion and particle size broadening in X-ray patterns. *Journal of applied physics*, *23*(4), 497-497.

[15] Hall, W. H., & Williamson, G. K. (1951). The diffraction pattern of cold worked metals: I the nature of extinction. *Proceedings of the Physical Society. Section B*, *64*(11), 937.

[16] Wilson, A. J. C. (1987). Functional form of some ideal hypersymmetric distributions of structure factors. *Acta Crystallographica Section A: Foundations of Crystallography*, *43*(4), 554-556.

[17] Dubey, S. K., Sharma, S., Pandey, S., & Diwakar, A. K. (2021). Structural Characterization and Optical Properties of Monoclinic $Ba_2MgSi_2O_7$ (BMS) Phosphor. *IJRPR*, 2(11), 327-332.

[18] Raman, C. V., & Krishnan, K. S. (1928). A new type of secondary radiation. *Nature*, *121*(3048), 501-502.

[19] Sharma, S. K., Yoder Jr, H. S., & Matson, D. W. (1988). Raman study of some Melilites in crystalline and glassy states. *Geochimica et Cosmochimica Acta*, *52*(8), 1961-1967.

[20] Hanuza, J., Ptak, M., Mączka, M., Hermanowicz, K., Lorenc, J., & Kaminskii, A. A. (2012). Polarized IR and Raman spectra of $Ca_2MgSi_2O_7$, $Ca_2ZnSi_2O_7$ and $Sr_2MgSi_2O_7$ single crystals: Temperature-dependent studies of commensurate to incommensurate and incommensurate to normal phase transitions. *Journal of Solid State Chemistry*, *191*, 90-101.

[21] Sharma S., Dubey SK. (2022). Specific Role of Novel TL Material in Various Favorable Applications. *Insights in Mining Science & Technology,* 3(2), 555609. DOI: 10.19080/IMST.2022.03.555609.

[22] Dubey SK, Sharma S, Diwakar AK. (2021). Structural & thermal properties of monoclinic $Ba_2MgSi_2O_7$ (BMS) Phosphor. *IRJMETS*, 3(11), 677-682.

[23]Chen, R. (1969). Glow curves with general order kinetics. *Journal of the electrochemical society*, *116*(9), 1254.

[24]Yuan, Z. X., Chang, C. K., Mao, D. L., & Ying, W. (2004). Effect of composition on the luminescent properties of $Sr_4Al_{14}O_{25}$: Eu^{2+}, Dy^{3+} phosphors. *Journal of Alloys and Compounds*, *377*(1-2), 268-271.

[25]McKeever, S. W. (1988). *Thermoluminescence of solids* (Vol. 3). Cambridge University Press.

[25]Mashangva, M., Singh, M. N., & Singh, T. B. (2011). Estimation of optimal trapping parameters relevant to persistent luminescence. *Indian Journal of Pure & Applied Physics*, 49, 583-589.